

---

# Law of Neural Interaction: Depth–Width Shape, Interaction Efficiency, and Generalization

---

Wenjie Sun<sup>1</sup> Jinning Yang<sup>2</sup> Shuai Zhang<sup>3</sup> Mengnan Du<sup>1,†</sup>

<sup>1</sup>The Chinese University of Hong Kong, Shenzhen

<sup>2</sup>Shenzhen Institutes of Advanced Technology, Chinese Academy of Sciences

<sup>3</sup>New Jersey Institute of Technology

wenjie1835@ghmail.com, jinny-yang@outlook.com, sz457@njit.edu,  
mengnan@cuhk.edu.cn

<sup>†</sup>Corresponding author.

## Abstract

The guidance of scaling laws has increased the resource demands of modern large language models (LLMs), yet it remains questionable whether these models utilize resources effectively under a fixed budget. Previous research has proved superposition as a key contributor to loss. By leveraging the Neural Feature Ansatz, we extend superposition from parameter space to gradient space and define it as neural interaction. We find that under a fixed budget, good generalization is usually accompanied by efficient neural interactions, and the model can be placed in an efficient interaction interval by adjusting its depth-width ratio ( $R_{D/W}$ ). In addition, as the budget scales up, the efficient interaction interval of the model remains relatively stable. By comparing existing small scale dense LLMs, we observe that models operating near this interval tend to perform better on the MMLU-Pro benchmark. Our findings reveal that the  $R_{D/W}$  influences resource utilization efficiency and thereby affects generalization, providing insights into model shape initialization and the understanding of model generalization mechanisms. Code for Neural Interaction Law is available at: [https://anonymous.4open.science/r/Neural\\_Interaction\\_Law-D788](https://anonymous.4open.science/r/Neural_Interaction_Law-D788).

## 1 Introduction

Scaling has become the dominant paradigm for modern machine learning. In language modeling, performance improves predictably as model size, dataset size, and compute increase, giving rise to empirical scaling laws that have shaped the design of contemporary large language models (LLMs) [1–4]. Subsequent work further argued that compute-optimal training requires scaling model parameters and training tokens in roughly equal proportion, suggesting that many models are undertrained relative to their size [5–8]. The findings collectively establish a compelling framework for advancement: larger models trained on more data tend to generalize better. However, they also raise a more fundamental question: if scaling laws achieve performance by allocating more parameters and data budgets, then how effectively networks utilize these resources under fixed resource budgets? Resolving this question is crucial for addressing the resource demands of modern LLMs and for understanding the generalization mechanisms of neural networks.

Existing explanations of scaling laws primarily include asymptotic statistics, geometry, training dynamics, and feature learning [9–13]. However, these perspectives mainly explain scaling in terms of asymptotic behavior, data geometry, or optimization, and say less about how limited representational resources are organized inside trained networks. Recently, Liu et al. [14] proposed an explanation grounded in representation: neural scaling may be driven by superposition. Under this

framework, models pack more features than available representational dimensions, so that interference among overlapping representations may become an important contributor to loss. This superposition perspective is compelling because it shifts the focus from raw capacity to representational efficiency. In terms of mathematics, this interference manifests as off-diagonal structure in the feature interaction matrix  $W^\top W$ . However, its current formulation relies on toy models constrained by a single hidden layer and tied weights, making it difficult to generalize to deep multilayer networks or other architectures [15–18].

To bridge this gap, we turn to the Neural Feature Ansatz (NFA). Radhakrishnan et al. [19] demonstrated that the Average Gradient Outer Product (AGOP) captures the features learned by neural networks. From this viewpoint, NFA links the feature geometry in the weight space to gradient space through AGOP, providing an architecture-agnostic route from the original weight-based intuition behind superposition to a quantity that can be measured in deep networks [19, 20]. In this work, we generalize superposition into the notion of gradient superposition, or more broadly, neural interaction, defined through the off-diagonal structure of AGOP. We quantify this interaction using two complementary metrics: the AGOP Off-diagonal Frobenius Energy (AOFE) for the absolute interactive energy, and the AOFE-ratio for the fraction of the network’s total sensitivity contributed by interaction. This allows us to move from asking whether interaction exists to asking whether it is efficient.

To study interaction efficiency under fixed budgets, we need a controlled way to redistribute limited resources, and the model’s structure (depth and width) naturally offers a choice. We find that, under fixed budgets, generalization is strongly associated with interaction efficiency, which can be systematically reshaped by the depth-width ratio ( $R_{D/W}$ ). The best generalizing configurations typically achieve a high interaction contribution (high AOFE-ratio) with a low absolute interaction energy (low AOFE), a regime we refer to as **benign superposition**. Based on these observations, we propose the **Law of Neural Interaction**: under fixed budgets, generalization depends not only on how much capacity a network has, but also on how efficiently it converts limited representational resources into reusable structure shared across inputs. From this perspective, depth and width matter because they reshape interaction efficiency in different ways, trading off compositional hierarchy against parallel representational freedom, so that the optimal model shape is not an isolated hyperparameter choice, but an architectural signature of efficient neural interaction. Our core contributions include:

- We generalize the definition of superposition to multilayer networks and arbitrary architectures through NFA and AGOP, defining it as "neural interaction". We propose two complementary metrics to quantify this interaction: absolute interaction energy (AOFE) and interaction contribution (AOFE-ratio). Based on the replication results of the Double Descent experiment, we propose the Law of Neural Interaction: under a fixed budget, generalization depends not only on the model’s capacity, but also on the efficiency with which it converts parameters into reusable feature structures.
- By fixing the budget across different network architectures and sweeping various depth-to-width ratios, we find that tuning a network’s depth-width shape can directly impact interaction efficiency, thereby indirectly affecting generalization. Furthermore, an interaction efficient interval exists under a fixed budget.
- Empirically, by scaling up parameter and data budgets, we find that this interaction efficient interval remains relatively stable. Additionally, by comparing existing small dense LLMs, we observe that models closer to this interval generally perform better on the MMLU-Pro benchmark.

## 2 Preliminaries

### 2.1 Neural Feature Ansatz (NFA)

A central perspective on feature learning is provided by the NFA [19], which posits that the feature geometry learned by a network layer is encoded in a neural feature matrix (NFM), and that this matrix is proportional to a positive power of the corresponding AGOP. Specifically, consider a trained network, a layer  $l$  with weight matrix  $W^{(l)}$ , and the corresponding local input  $u^{(l)}$ . The NFA states that

$$W^{(l)\top} W^{(l)} \propto \left( \frac{1}{N} \sum_{p=1}^N \nabla_{u^{(l)}} \hat{f}(\mathbf{x}^{(p)}) \nabla_{u^{(l)}} \hat{f}(\mathbf{x}^{(p)})^\top \right)^\alpha, \quad (1)$$

where  $N$  is the number of samples and  $\alpha > 0$  is the exponent in the ansatz. For vector-valued outputs, we use the input-gradient matrix whose columns are the gradients of the output coordinates.

Equation (1) is central for our purposes because it connects the classical toy-model object  $W^\top W$  to the gradient-based operator AGOP. In the tied-weight toy model, the relevant NFM numerically coincides with  $W^\top W$ . However, the two viewpoints carry different interpretations. In the toy autoencoder model,  $W^\top W$  is used to measure overlap among feature directions in the bottleneck representation. By contrast, under the NFA viewpoint, the corresponding AGOP characterizes how different input directions jointly influence the network output under the data distribution. Thus, although  $W^\top W$  and the NFM coincide in this special setting, the latter admits a gradient-based interpretation that naturally generalizes to untied and multilayer networks. By adopting the NFA viewpoint, we can reinterpret classical weight space superposition as a gradient space phenomenon. This allows us to move beyond the constraints of toy models and formally define a generalizable measure of feature entanglement, which we term "neural interaction" in the next section.

## 2.2 Gradient Superposition and Neural Interaction

Motivated by the NFA, we extend superposition from representation space to gradient space.

**Definition 1 (Gradient superposition).** Let  $f : \mathbb{R}^d \rightarrow \mathbb{R}^c$  be a network, and  $J_f(\mathbf{x}) \in \mathbb{R}^{d \times c}$  as the input-gradient matrix. We define the *input-space AGOP* of  $f$  under an input distribution  $\mathcal{D}$  as

$$\mathbf{G}_f(\mathcal{D}) = \mathbb{E}_{\mathbf{x} \sim \mathcal{D}} [J_f(\mathbf{x})J_f(\mathbf{x})^\top] \in \mathbb{R}^{d \times d}. \quad (2)$$

We say that  $f$  exhibits *gradient superposition* on  $\mathcal{D}$  if  $\mathbf{G}_f(\mathcal{D})$  is not diagonal; equivalently, if there exist  $i \neq j$  such that

$$(\mathbf{G}_f(\mathcal{D}))_{ij} \neq 0. \quad (3)$$

This definition captures the idea that different input directions affect the output in a coupled, non-independent manner. In particular, the off-diagonal entry  $(\mathbf{G}_f(\mathcal{D}))_{ij}$  measures the average co-sensitivity of the output to perturbations along the  $i$ -th and  $j$ -th input directions. If the relevant directions are disentangled in the chosen basis, then  $\mathbf{G}_f(\mathcal{D})$  is close to diagonal in that basis. Conversely, substantial off-diagonal mass indicates that the model relies on coupled input directions and therefore exhibits strong gradient superposition. Throughout the paper, we also use the broader term *neural interaction* to refer to this gradient-mediated coupling structure.

To quantify the strength of this effect, we introduce the *AGOP Off-diagonal Frobenius Energy* (AOFE):

$$\text{AOFE}(f, \mathcal{D}) = \|\mathbf{G}_f(\mathcal{D}) - \text{diag}(\mathbf{G}_f(\mathcal{D}))\|_F^2 = \sum_{i \neq j} (\mathbf{G}_f(\mathcal{D}))_{ij}^2. \quad (4)$$

AOFE measures the total off-diagonal energy of AGOP, and therefore captures the absolute strength of cross-directional gradient coupling.

To normalize this quantity by the total sensitivity of the network, we further define the *AOFE-ratio*:

$$\text{AOFE-Ratio}(f, \mathcal{D}) = \frac{\|\mathbf{G}_f(\mathcal{D}) - \text{diag}(\mathbf{G}_f(\mathcal{D}))\|_F^2}{\|\mathbf{G}_f(\mathcal{D})\|_F^2} = \frac{\sum_{i \neq j} (\mathbf{G}_f(\mathcal{D}))_{ij}^2}{\sum_{i,j} (\mathbf{G}_f(\mathcal{D}))_{ij}^2}. \quad (5)$$

AOFE-ratio measures the fraction of total AGOP energy carried by off-diagonal coupling. While AOFE quantifies the *absolute cost* of interaction, AOFE-ratio quantifies its relative contribution to the overall sensitivity structure of the network.

In summary, AOFE and AOFE-ratio provide complementary information: the former measures how much interaction energy the network expends, while the latter measures how much of the network's total sensitivity is interaction-driven. Their combination will serve as our notion of *interaction efficiency* in the remainder of the paper.

This definition recovers the classical toy-model intuition through the NFA bridge. In the tied-weight setting, the off-diagonal structure of  $W^\top W$  corresponds to the off-diagonal structure of the associated NFM/AGOP, while AOFE and AOFE-ratio remain well-defined for untied, deep, and heterogeneous architectures. This makes them natural quantities to track in the more general settings considered later in the paper.

### 3 Double Descent Example

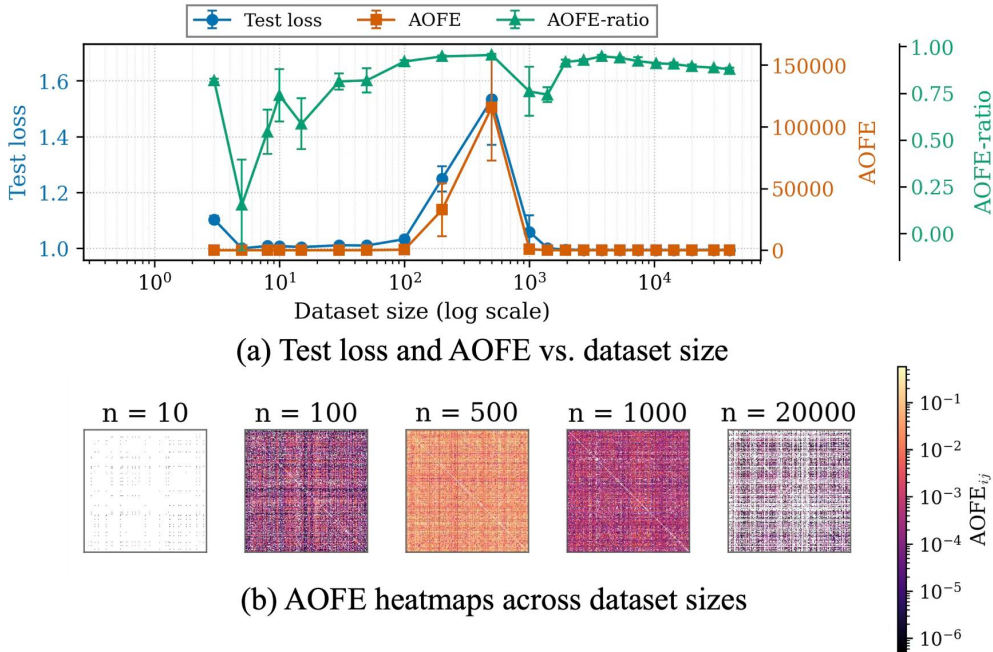


Figure 1:  $\mathcal{L}_{\text{test}}$ , AOFE, and AOFE-ratio across dataset sizes. (a)  $L_{\text{test}}$  and AOFE as functions of training set size. (b) AOFE-ratio as a function of training set size. (c) Representative AGOP heatmaps at selected training set sizes.

Liu et al. [14] argue that loss can arise from interference between features induced by superposition. Through the NFA, such parameter space interference has a gradient space counterpart: the geometry of learned features can be captured by AGOP. We therefore use the classical bottleneck double descent setting to ask whether AOFE and AOFE-ratio track the transition from memorization to feature learning [17]. The purpose of this setting is that by adjusting the degree of overparameterization, it spans different learning regimes, which allows us to observe the differences in interactions across these regimes.

**Experiment Setup.** We use the tied toy autoencoder to reproduce the Anthropic double-descent setting [17]. Sweeping dataset sizes from small- $N$  settings to  $N = 40,000$ , keep the test distribution fixed, and average over multiple random seeds. For each dataset size, we evaluate  $L_{\text{test}}$  together with AOFE and AOFE-ratio. The model architecture and data generation procedure follow the standard setup (see Appendix B.1 for full details).

**Results.** During the first descent phase ( $N < 100$ ), the model achieves a low  $L_{\text{test}}$  even before forming a stable and efficient interaction pattern. For example, at  $N = 5$ ,  $L_{\text{test}} \approx 0.999$  while the AOFE ratio is only  $\approx 0.15$ , as shown in Figure 1(a). More broadly, the AOFE-ratio exhibits no correlation with  $L_{\text{test}}$  in the low data regime. This is consistent with a memorization dominated mechanism: because the model is highly overparameterized, simply memorizing the data points can also achieve low  $L_{\text{test}}$ .

Unlike the first descent, when  $N$  increases beyond the interpolation threshold, both  $L_{\text{test}}$  and AOFE drop sharply, but the AOFE-ratio begins to saturate, especially in the large data regime ( $N \gtrsim 2000$ ). This suggests that the second descent corresponds to the network allocating a substantial portion of its sensitivity to coupled directions, i.e., interaction features.

The difference in the AOFE-ratio between the two descent phases indicates that in the memorization phase, the neural network’s sensitivity is concentrated more on the diagonal elements of the AGOP,

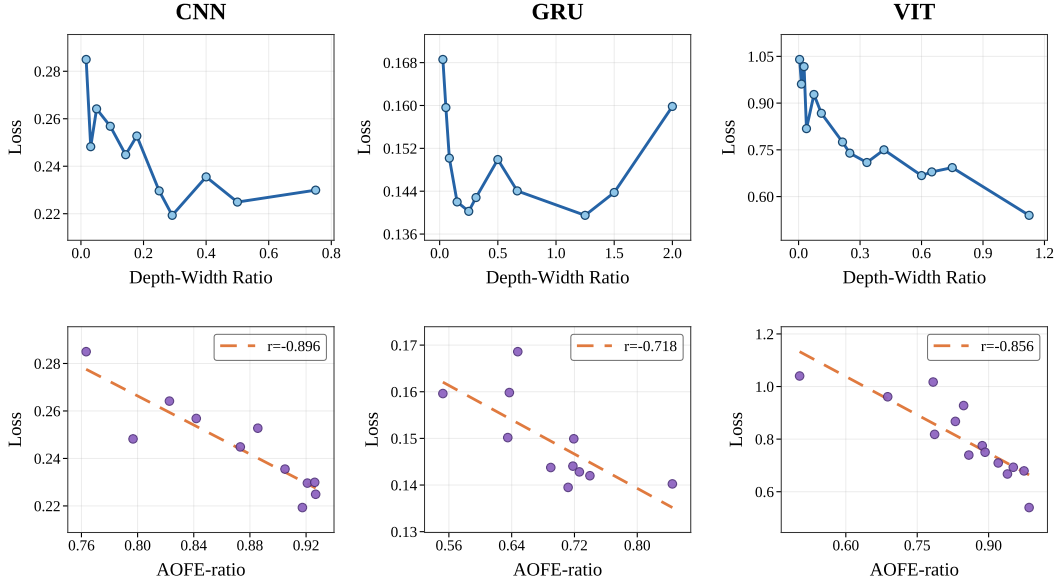


Figure 2: Cross-Network fixed budget shape sweeps. Top row: test loss versus  $R_{D/W}$  for CNN, GRU, and ViT. Bottom row: test loss versus AOFE-ratio.

while the off-diagonal elements of the AGOP remain sparse, as seen in the first heatmap of Figure 1(b). In the feature learning phase, due to a lower degree of over-parameterization, the network cannot memorize all data points and is forced to learn efficient, reusable information across different inputs. Consequently, the network’s sensitivity is increasingly carried by the off-diagonal elements of the AGOP. Interestingly, throughout the entire process, AOFE and  $L_{\text{test}}$  exhibit a highly consistent correlation, with a Pearson correlation coefficient as 0.94. We attribute this to the NFA connecting parameter space and gradient space. Since gradient descent and weight decay favor low-norm parameter solutions to maximize the degrees of freedom in the solution space, AOFE indirectly measures the degrees of freedom in that space [21, 22].

From this perspective, one of Chinchilla’s key contributions is to constrain the over-parameterization of the network to a regime where feature learning can occur efficiently, i.e., where interaction features dominate generalization [5]. Therefore, we argue that good generalization arises when the network achieves a high AOFE-ratio with a low AOFE, a state we term *benign superposition*. This motivates studying whether network shape, under a fixed budget, can similarly improve interaction efficiency.

## 4 Cross-Network Verification

### 4.1 Experimental Setup

The double-descent experiment suggests that efficient interaction is not merely the presence of off-diagonal AGOP structure, but the allocation of a large fraction of sensitivity to reusable interaction while keeping the absolute cost controlled. We now ask whether this signal persists beyond the tied toy model. To this end, we perform fixed parameter depth-width sweeps on three architecture/task pairs: a residual CNN on SVHN, a small ViT on SVHN [23], and a multi-layer GRU on a synthetic temporal-interaction task. In each sweep, the parameter budget is fixed and the width is chosen as a function of depth so that all shapes remain approximately budget matched. After training, we evaluate  $L_{\text{test}}$  and the interaction metrics from Section 2.2 at the best validation checkpoint. Unless otherwise stated, AGOP estimates use 2048 examples, exact gradients, centered logits, and logit RMS normalization. Further architectural and optimization details are given in Appendix B.2.

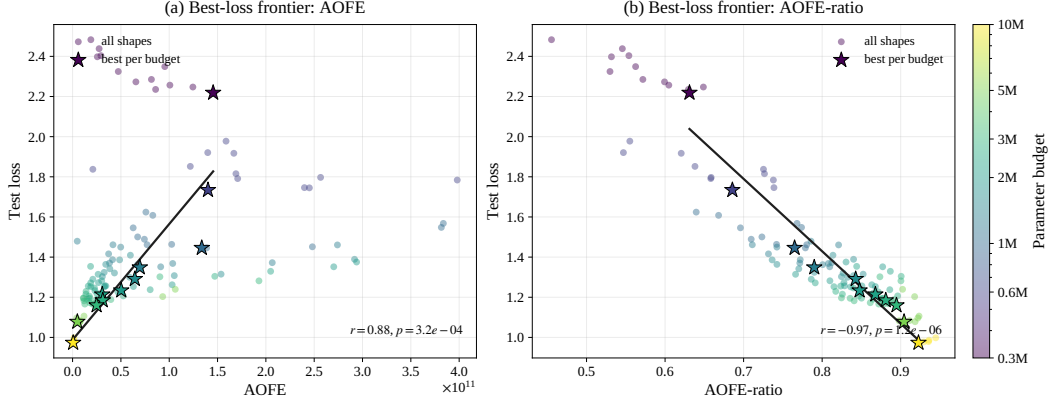


Figure 3: Budget-wise best points in the Tiny Transformer shape sweep. Left:  $L_{test}$  versus AOFE. Right:  $L_{test}$  versus AOFE-ratio. Circles denote all scanned shapes and stars denote the best-loss shape at each budget. Color indicates parameter budget.

## 4.2 Results and Analysis

Figure 2 shows that the negative relation between  $L_{test}$  and AOFE-ratio persists across the three architecture/task pairs. For the CNN sweep at  $P = 500k$ ,  $L_{test}$  and AOFE-ratio exhibit a strong negative correlation, with Pearson  $r = -0.896$ . The best performing region occurs around an intermediate  $R_{D/W}$ ,  $R_{D/W} \approx 0.29$ , where the model attains the lowest  $L_{test}$  and one of the highest AOFE-ratio. For the ViT sweep at the same parameter budget, the relation is also strongly negative, with Pearson  $r = -0.856$ . Unlike the CNN case, the ViT loss continues to decrease toward the deepest scanned model, suggesting that the right boundary of its efficient interaction interval is not resolved within the present scan. For the GRU temporal interaction task,  $L_{test}$  and AOFE-ratio again show a negative correlation, with Pearson  $r = -0.718$ . The lowest  $L_{test}$  model lies in a pre degradation regime, whereas further increasing depth degrades performance, indicating that recurrent models also exhibit a bounded efficient shape range. Detailed results can be found in the Table 2.4 and 3 of Appendix C.2.

These results suggest that the relationship between efficient neural interactions and generalization holds across networks and tasks. Within a fixed budget, we can modulate the distribution of parameters across depth and width to affect interactions, thereby identifying the interval for efficient neural interactions. They also suggest that depth and width not only determine model size but also shape how limited resources are organized. Width provides independent representational directions, and depth repeatedly recomposes these directions into higher-order structures. When a model is too shallow and too wide, features may remain weakly coupled; when it is too deep and too narrow, interactions are forced to proceed through compressed representations, incurring high costs. This also explains why the AOFE-ratio closely correlates with generalization capability. Inspired by Chinchilla [5], modern LLMs constrain their overparameterization within the feature learning regime, compelling the model to seek reusable information across samples, i.e., features. In AGOP, such reusable information manifests as coupling sensitivity across different inputs, and the AOFE-ratio measures the proportion of total sensitivity carried by these couplings. Therefore, a higher AOFE-ratio indicates that the network is more efficiently utilizing its capacity to encode reusable feature interactions. The generality of the law of neural interaction suggests that, although different architectures process images, temporal sequences, and text in different ways, they face the same fixed budget problem: how to convert parameters into reusable interaction structures. In this sense, the depth-width shape acts as a general mechanism for controlling interaction efficiency, linking architectural resource allocation to generalization.

## 5 Language Models

### 5.1 Budget Sweep

To investigate how the  $R_{D/W}$  of the model changes with increasing parameter budget, we trained decoder-only Tiny Transformers on the WikiText-103 dataset across eleven budgets ranging from 0.3M to 10M parameters. For each budget  $N$ , we searched over a predefined set of depths to identify the largest  $d_{\text{model}}$  that satisfies the budget constraint while ensuring  $d_{\text{model}}$  is an integer multiple of the fixed head dimension. We then fixed the head dimension at  $d_{\text{head}} = 4$  and set the number of attention heads adaptively according to  $n_{\text{head}} = d_{\text{model}}/d_{\text{head}}$ . This procedure keeps the active parameter count as close as possible to the target budget. For each architecture, we recorded the  $L_{\text{test}}$ , AOFE, and AOFE-ratio; detailed implementation details are provided in Table 5, 7, 9 of Appendix B.3 and the detailed configurations and metrics for every budget are provided in Table 6, 8, 10 of Appendix C.3.

**Results.** Under a fixed budget, the  $L_{\text{test}}$  can be affected by adjusting the model’s  $R_{D/W}$ . Models with lower loss tend to exhibit higher AOFE-ratio, whereas their relationship with raw AOFE is less stable. This may be because AOFE measures the absolute magnitude of interaction energy, whose scale can be strongly affected by the overall budget. By contrast, AOFE-ratio directly quantifies the fraction of the model’s total sensitivity that is carried by interaction. Across the budget-wise best points,  $L_{\text{test}}$  shows a significant positive correlation with the corresponding AOFE, with Pearson  $r = 0.883$ , and a significant negative correlation with AOFE-ratio, with Pearson  $r = -0.967$ ; detailed trend can be found in Figure 3. This pattern is consistent with the feature-learning phase observed in the double-descent experiment. As the model budget increases, the model becomes increasingly capable of capturing reusable information shared across different inputs, and the fraction of total sensitivity carried by interaction rises. In other words, better language models achieve lower loss by using interaction more efficiently: they expend less interaction energy while capturing more general reusable information among different inputs.

The best loss shapes also reveal a stable depth-width preference. Excluding budgets below 1.0M, where outliers may arise because interaction efficiency has not yet fully emerged or the models remain underparameterized, the optimal  $R_{D/W}$  concentrate in the interval  $\alpha^* \in [0.023, 0.047]$ . The corresponding best shapes occupy an intermediate regime that balances depth and width. This observation suggests that the optimal  $R_{D/W}$  may be determined by three interacting factors: architecture, degree of overparameterization, and task. Once these factors are fixed, there may exist a range of  $R_{D/W}$  that maximizes interaction efficiency, within which the model can most effectively convert limited parameters into reusable structure.

### 5.2 External Comparison

To examine whether the  $R_{D/W}$  preference from our controlled TinyGPT sweep has external relevance, we compare contemporary small dense LLMs to the interaction efficient interval ( $0.023 \leq \alpha \leq 0.047$ ). This comparison is not a controlled validation, since public LLMs differ in tokenizer, data mixture, optimizer, compute, context length, instruction tuning, and post-training. Instead, it is used as an external sanity check: if the interval captures a meaningful architectural efficiency principle, models closer to it should tend to perform better within comparable parameter scales. We restrict the comparison to dense decoder-only models between 0.5B and 9B parameters, excluding MoE models because routing and active parameter effects make  $L/d_{\text{model}}$  less directly comparable. For each model, we collect  $d_{\text{model}}$ ,  $L$ , parameter count, and MMLU-Pro from public model cards, configuration files, Open LLM Leaderboard 2 entries, and benchmark summaries; duplicate shapes sharing the same  $(d_{\text{model}}, L)$  but differing mainly in post-training are removed. The detailed configurations are listed in Table 11. We define the distance to the TinyGPT interval as:

$$\Delta_\alpha = \max\left(\frac{L}{d_{\text{model}}} - 0.047, 0.023 - \frac{L}{d_{\text{model}}}, 0\right). \quad (6)$$

Thus,  $\Delta_\alpha = 0$  for models inside the interval, and larger values indicate greater deviation from the interaction-efficient interval. Figure 4(b) compares  $\Delta_\alpha$  with MMLU-Pro performance, grouped by parameter scale. The overall trend is negative: within comparable size ranges, models closer to the interval tend to obtain higher MMLU-Pro scores. The trend is strongest in the 1–2.5B group ( $r = -0.84$ ), remains negative but weaker in the 3–4.5B group ( $r = -0.42$ ), and becomes weak

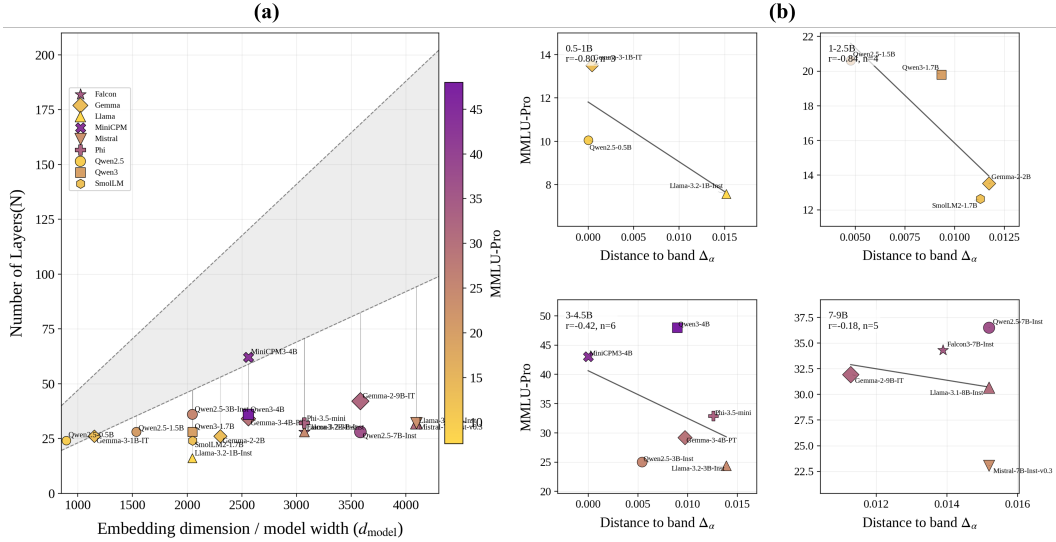


Figure 4:  $R_{D/W}$  distance and MMLU-Pro performance in small dense LLMs. (a)  $R_{D/W}$  of contemporary small dense LLMs. The shaded region denotes the interaction-efficient interval ( $0.023 \leq L/d_{\text{model}} \leq 0.047$ ), color indicates MMLU-Pro. (b) MMLU-Pro versus distance to the interval, grouped by parameter scale, with fitted linear trends within each group.

in the 7–9B group ( $r = -0.18$ ). The weakening at larger scales is expected, because many models in this interval have similar wide shallow shapes, reducing the dynamic range of  $\Delta_\alpha$ , while data mixture, instruction tuning, and reasoning-oriented post-training increasingly dominate benchmark differences. The 0.5–1B group also shows a negative trend ( $r = -0.80$ ), but contains only three models and should be interpreted qualitatively.

These observations support a cautious version of the  $R_{D/W}$  hypothesis. The controlled sweep shows that dense decoder-only Transformers can have a stable interaction efficient depth-width interval. The external LLM comparison suggests that proximity to this interval is directionally associated with stronger MMLU-Pro performance among small dense models. However,  $\Delta_\alpha$  should not be treated as an independent predictor of benchmark performance. It is better understood as a coarse architectural covariate: it reflects whether a model shape is likely to allocate its fixed parameter budget in a way that supports efficient neural interaction. Together, the TinyGPT sweep and small LLM comparison extend the Law of Neural Interaction to language modeling. Under fixed or comparable budgets, generalization depends not only on scale, but also on whether depth and width organize that scale into efficient, reusable interaction structure.

## 6 Related Work

### 6.1 Neural Scaling Law

As an empirical principle in deep learning, Neural Scaling Laws describe the predictable power-law improvements in neural network performance as model parameter count, dataset size, and training compute increase. This empirical law was initially discovered by Hestness et al. [2] in large-scale experiments spanning tasks such as machine translation, language modeling, and image classification. Sharma and Kaplan [24] further extended these observations to Transformer-based language models, establishing the key finding that loss scales as a power law with respect to model size, dataset size, and compute. The discovery of scaling laws has not only substantially optimized compute and data allocation strategies in model training but has also triggered extensive theoretical exploration into their underlying mechanisms.

Sharma and Kaplan [24], Bahri et al. [10], and Bordelon et al. [9] approached the issue from the perspectives of data geometry and kernel theory, attributing the scaling exponents to the intrinsic dimensionality of the data manifold and the spectral properties of the data covariance. Bordelon et al.

[9] and Song et al. [25] argued that the macroscopic power-law decay originates from the model’s sequential mastery of discrete features or skills, proposing the “Quantization Model” and “Resource Model,” respectively. Liu et al. [14] noted that existing explanatory frameworks generally assume the absence of feature interference, corresponding to the weak superposition regime, and suggested that loss may arise from strong superposition of features packed into dimension-constrained spaces. This perspective offers fresh insights for understanding scaling laws. However, current explanations predominantly focus on parameter count and fail to address Kaplan et al. [1]’s notable observation: when the total number of parameters is held fixed, loss exhibits a high degree of invariance to the allocation between depth and width. Up to now, this phenomenon continues to be regarded primarily as an empirical regularity rather than a consequence of deeper principles. The rest of the related work can be found in Appendix A.

## 7 Discussion

The central result of this work is that, under a fixed parameter budget, strong generalization is characterized not by more or fewer neural interactions, but by a regime we term *benign superposition*: the network achieves a high fraction of interaction driven sensitivity (high AOFE-ratio) while keeping the absolute interaction energy low (low AOFE). This pattern recurs across architectures. In the CNN, GRU, and ViT shape sweeps, lower-loss configurations consistently exhibit a higher AOFE-ratio. In contrary, the AOFE tracks scale and overparameterization more closely. A possible explanation is that raw AOFE partly inherits an imprint of the low-norm solutions favored by gradient descent and weight decay [22, 26], it confounds meaningful interaction with the strength of the optimization constraint. Normalizing by total sensitivity removes that scale artifact, making AOFE-ratio a cleaner measure of how the network allocates its limited representational resources to reusable structure. Thus, under a fixed budget, the AOFE-ratio serves as a more direct diagnostic of interaction efficiency, while AOFE is better suited for comparing across budgets.

The  $R_{D/W}$  operates directly on this efficiency. Width supplies parallel representational freedom: in the infinite width setting, optimization becomes stable but nearly linear, with weakly coupled features that contribute little to cross input reuse [27]. Depth enforces composition across layers, repackaging features into higher-order structure. In our experiments, networks that are too shallow and wide fail to develop sufficient interaction contribution (low AOFE-ratio), while networks that are too deep and narrow drive up the absolute cost of interaction (high AOFE) without a commensurate gain in contribution. The optimal depth-width configurations occupy an intermediate regime where the ratio of contribution to cost is maximized. Under a controlled sweep of TinyGPT models, the shapes that minimize loss concentrate in the interval  $0.023 \leq L/d_{\text{model}} \leq 0.047$ . When we compare existing small dense LLMs against this band, we observe that models closer to the interval tend to score higher on MMLU-Pro, particularly in the 1-2.5B parameter group. We do not interpret this interval as an independent performance predictor. It is better understood as a coarse architectural covariate: it signals whether the model shape, before any post-training intervention, is aligned with the structural conditions for efficient neural interaction. The correlation weakens at larger scales, as data mixture, instruction tuning, and reasoning-oriented fine-tuning increasingly dominate benchmark differences. Meanwhile, the difference between the empirical shapes of contemporary LLMs and our identified interval highlights a potential inefficiency in current scaling paradigms. While modern models rigorously optimize the allocation of parameter and allocation, their  $R_{D/W}$  are often dictated by hardware constraints or empirical rules rather than representational efficiency. Consequently, many models may underutilize their fixed parameter and data budgets.

Although the main limitation of this work is scale, the interval was obtained from byte-level TinyGPT models up to 10M parameters, and its direct numerical transfer to billion-parameter LLMs would be premature. What the interval provides is a theoretical signpost. It suggests that the next step in understanding neural scaling is not simply refining the balance between parameters and data, but characterizing how architecture organizes those resources into an efficient interaction structure. Future work should track AOFE and AOFE-ratio throughout training in larger controlled Transformers to test and refine this hypothesis. Taken together, the law of neural interaction reframes fixed budget generalization as a resource organization problem: the best models achieve high relative interaction contribution while keeping absolute interaction energy under control.

## References

- [1] Kaplan, J., McCandlish, S., Henighan, T., Brown, T. B., Chess, B., Child, R., Gray, S., Radford, A., Wu, J., & Amodei, D. (2020) Scaling laws for neural language models. *arXiv preprint arXiv:2001.08361*
- [2] Hestness, J., Narang, S., Ardalani, N., Diamos, G., Jun, H., Kianinejad, H., Patwary, M. M. A., Yang, Y., & Zhou, Y. (2017) Deep learning scaling is predictable, empirically. *arXiv preprint arXiv:1712.00409*
- [3] Rosenfeld, J. S., Rosenfeld, A., Belinkov, Y., & Shavit, N. (2019) A constructive prediction of the generalization error across scales. *arXiv preprint arXiv:1909.12673*
- [4] Brown, T., Mann, B., Ryder, N., Subbiah, M., Kaplan, J. D., Dhariwal, P., Neelakantan, A., Shyam, P., Sastry, G., Askell, A., & others (2020) Language models are few-shot learners. *Advances in neural information processing systems* **33**:1877–1901.
- [5] Hoffmann, J., Borgeaud, S., Mensch, A., Buchatskaya, E., Cai, T., Rutherford, E., Casas, D., Hendricks, L. A., Welbl, J., Clark, A., & others (2022) Training compute-optimal large language models. *arXiv preprint arXiv:2203.15556* **10**.
- [6] Hernandez, D., Kaplan, J., Henighan, T., & McCandlish, S. (2021) Scaling laws for transfer. *arXiv preprint arXiv:2102.01293*
- [7] Ghorbani, B., Firat, O., Freitag, M., Bapna, A., Krikun, M., Garcia, X., Chelba, C., & Cherry, C. (2021) Scaling laws for neural machine translation. *arXiv preprint arXiv:2109.07740*
- [8] Alabdulmohsin, I. M., Neyshabur, B., & Zhai, X. (2022) Revisiting neural scaling laws in language and vision. *Advances in Neural Information Processing Systems* **35**:22300–22312.
- [9] Bordelon, B., Atanasov, A., & Pehlevan, C. (2024) A dynamical model of neural scaling laws. *arXiv preprint arXiv:2402.01092*
- [10] Bahri, Y., Dyer, E., Kaplan, J., Lee, J., & Sharma, U. (2024) Explaining neural scaling laws. *Proceedings of the National Academy of Sciences* **121**(27):e2311878121.
- [11] Sorscher, B., Geirhos, R., Shekhar, S., Ganguli, S., & Morcos, A. (2022) Beyond neural scaling laws: beating power law scaling via data pruning. *Advances in Neural Information Processing Systems* **35**:19523–19536.
- [12] Hutter, M. (2021) Learning curve theory. *arXiv preprint arXiv:2102.04074*
- [13] Bordelon, B., Atanasov, A., & Pehlevan, C. (2025) How feature learning can improve neural scaling laws. *Journal of Statistical Mechanics: Theory and Experiment* **2025**(8):084002.
- [14] Liu, Y., Liu, Z., & Gore, J. (2025) Superposition yields robust neural scaling. *arXiv preprint arXiv:2505.10465*
- [15] Elhage, N., Hume, T., Olsson, C., Schiefer, N., Henighan, T., Kravec, S., Hatfield-Dodds, Z., Lasenby, R., Drain, D., Chen, C., & others (2022) Toy models of superposition. *arXiv preprint arXiv:2209.10652*
- [16] Cunningham, H., Ewart, A., Riggs, L., Huben, R., & Sharkey, L. (2023) Sparse autoencoders find highly interpretable features in language models. *arXiv preprint arXiv:2309.08600*
- [17] Henighan, T., Carter, S., Hume, T., Elhage, N., Lasenby, R., Fort, S., Schiefer, N., & Olah, C. (2023) Superposition, memorization, and double descent. *Transformer Circuits Thread* **6**(24):1725–1744.
- [18] Elhage, N., Lasenby, R., & Olah, C. (2023) Privileged bases in the transformer residual stream. *Transformer Circuits Thread* **24**.
- [19] Radhakrishnan, A., Beaglehole, D., Pandit, P., & Belkin, M. (2024) Mechanism for feature learning in neural networks and backpropagation-free machine learning models. *Science* **383**(6690):1461–1467.
- [20] Tansley, E., Massart, E., & Cartis, C. (2025) On the neural feature ansatz for deep neural networks. *arXiv preprint arXiv:2510.15563*
- [21] d’Angelo, F., Andriushchenko, M., Varre, A., & Flammarion, N. (2024) Why do we need weight decay in modern deep learning? *Advances in Neural Information Processing Systems* **37**:23191–23223.
- [22] Soudry, D., Hoffer, E., Nacson, M. S., Gunasekar, S., & Srebro, N. (2018) The implicit bias of gradient descent on separable data. *Journal of Machine Learning Research* **19**(70):1–57.

- [23] Netzer , Y., Wang , T., Coates , A., Bissacco , A., Wu , B., Ng , A. Y., & others (2011) Reading digits in natural images with unsupervised feature learning. In *NIPS workshop on deep learning and unsupervised feature learning 2011*, pp. 4. Granada.
- [24] Sharma , U. & Kaplan , J. (2022) Scaling laws from the data manifold dimension. *Journal of Machine Learning Research* **23**(9):1–34.
- [25] Song , J., Liu , Z., Tegmark , M., & Gore , J. (2024) A resource model for neural scaling law. *arXiv preprint arXiv:2402.05164*
- [26] Gunasekar , S., Woodworth , B. E., Bhojanapalli , S., Neyshabur , B., & Srebro , N. (2017) Implicit regularization in matrix factorization. *Advances in neural information processing systems* **30**.
- [27] Jacot , A., Gabriel , F., & Hongler , C. (2018) Neural tangent kernel: Convergence and generalization in neural networks. *Advances in neural information processing systems* **31**.
- [28] Gao , L., Tour , T. D., Tillman , H., Goh , G., Troll , R., Radford , A., Sutskever , I., Leike , J., & Wu , J. (2024) Scaling and evaluating sparse autoencoders. *arXiv preprint arXiv:2406.04093*
- [29] Lieberum , T., Rajamanoharan , S., Conmy , A., Smith , L., Sonnerat , N., Varma , V., Kramár , J., Dragan , A., Shah , R., & Nanda , N. (2024) Gemma scope: Open sparse autoencoders everywhere all at once on gemma 2. In *Proceedings of the 7th BlackboxNLP Workshop: Analyzing and Interpreting Neural Networks for NLP* pages 278–300.
- [30] Sun , W., Wang , D., & Hu , L. () The price of amortized inference in sparse autoencoders. In *The Fourteenth International Conference on Learning Representations*
- [31] Lawson , T., Farnik , L., Houghton , C., & Aitchison , L. (2024) Residual stream analysis with multi-layer saes. *arXiv preprint arXiv:2409.04185*
- [32] Balagansky , N., Maksimov , I., & Gavrilo , D. (2024) Mechanistic permutability: Match features across layers. *arXiv preprint arXiv:2410.07656*
- [33] Lindsey , J., Templeton , A., Marcus , J., Conerly , T., Batson , J., & Olah , C. (2024) Sparse crosscoders for cross-layer features and model diffing. *Transformer Circuits Thread* pages 3982–3992.
- [34] Shi , W., Li , S., Liang , T., Wan , M., Ma , G., Wang , X., & He , X. (2025) Route sparse autoencoder to interpret large language models. In *Proceedings of the 2025 Conference on Empirical Methods in Natural Language Processing* pages 6812–6826.
- [35] Hanna , M., Piotrowski , M., Lindsey , J., & Ameisen , E. (2025) Circuit-tracer: A new library for finding feature circuits. In *Proceedings of the 8th BlackboxNLP Workshop: Analyzing and Interpreting Neural Networks for NLP* pages 239–249.
- [36] Beaglehole , D., Súkeník , P., Mondelli , M., & Belkin , M. (2024) Average gradient outer product as a mechanism for deep neural collapse. *Advances in Neural Information Processing Systems* **37**:130764–130796.
- [37] Radhakrishnan , A., Beaglehole , D., Pandit , P., & Belkin , M. (2022) Mechanism of feature learning in deep fully connected networks and kernel machines that recursively learn features. *arXiv preprint arXiv:2212.13881*
- [38] Frankle , J. & Carbin , M. (2018) The lottery ticket hypothesis: Finding sparse, trainable neural networks. *arXiv preprint arXiv:1803.03635*
- [39] Mallinar , N., Beaglehole , D., Zhu , L., Radhakrishnan , A., Pandit , P., & Belkin , M. (2024) Emergence in non-neural models: grokking modular arithmetic via average gradient outer product. *arXiv preprint arXiv:2407.20199*

## A More Related Work

### A.1 Superposition Hypothesis

The superposition hypothesis was originally introduced to explain the phenomenon of neuron polysemanticity, where a single neuron usually activates to multiple different concepts[15]. This hypothesis posits that polysemanticity arises from the limited width of neural networks, which forces different features to be encoded in non-orthogonal directions within the activation space. Liu et al. [14] provided the first rigorous confirmation of this phenomenon by examining the off-diagonal elements of the product of encoder and decoder weight in a toy model (an autoencoder). This discovery also catalyzed a large amount of subsequent research aimed at resolving polysemanticity through the use of Sparse Autoencoders (SAEs)[28, 16, 29, 30].

While toy models established that superposition of representations occurs within single-layer networks, the existence of cross-layer superposition, along with effective methods for observing and quantifying it, remains an open question. Moreover, because SAEs are trained independently on each layer, their ability to address cross-layer phenomena is inherently limited[31, 32]. Subsequent work on cross-layer superposition has given rise to several important extensions. For instance, Lindsey et al. trained a single jointly encoding and reconstructing SAE on activation vectors from all layers, with the explicit goal of capturing cross-layer shared features; they termed this architecture the Crosscoder[33]. Shi et al. [34] further proposed RouteSAE, which employs a lightweight routing mechanism to dynamically integrate multi-layer activations. Their analysis revealed that low-level features tend to peak in early layers, whereas high-level features become increasingly prominent in later layers. Additionally, Anthropic’s open-source circuit tracer tracks the inter-layer evolution of features by shifting the SAE reconstruction target from the activations of the current layer to those of the subsequent layer[35]. Although these studies are constrained by the inconsistency issues inherent to the non-convex optimization of SAEs, they collectively provide compelling evidence for the existence of cross-layer superposition. Nevertheless, the challenge of accurately observing and quantifying such cross-layer phenomena has yet to be fully resolved.

### A.2 Neural Feature Ansatz (NFA)

Understanding how neural networks learn task-relevant features has long been a fundamental open problem. In a landmark contribution, Radhakrishnan et al. [19] proposed the average gradient outer product (AGOP) as a unifying mathematical mechanism for feature learning in neural networks. They demonstrated that, upon convergence of training in deep neural networks, the Gram matrix of the layer weights is proportional to the AGOP of the output with respect to the input, and formalized this regularity as the NFA. A major insight of the NFA is that it establishes feature learning as a universal principle that is not confined to backpropagation or any specific neural architecture, but holds across diverse networks and tasks. Building upon the NFA mechanistic framework, subsequent studies have leveraged this principle to illuminate a series of complex network phenomena, including deep neural collapse[36], the emergence of spurious features and simplicity bias[37], pruning dynamics related to the Lottery Ticket Hypothesis[38], and grokking[39]. The success of NFA highlights that neural networks essentially capture task-relevant features by aligning their weights with the gradient outer product, thereby providing a general bridge connecting training dynamics and feature geometry. In this paper, we extend the definition of superposition from a gradient perspective based on NFA theory, enabling a formal understanding of the shape-independence phenomenon in neural scaling laws.

## B Experimental Details

### B.1 Double Descent

We use a tied two-layer bottleneck reconstruction model to reproduce the double-descent setting. Each input vector  $\mathbf{x} \in \mathbb{R}^d$  has dimension  $d = 1000$ . The hidden bottleneck dimension is fixed to  $m = 2$ . Let  $\mathbf{W} \in \mathbb{R}^{m \times d}$  denote the encoder weight. The model is

$$\hat{\mathbf{x}} = f(\mathbf{x}) = \text{ReLU}(\mathbf{W}^\top \mathbf{W}\mathbf{x} + \mathbf{b}), \tag{7}$$

where  $\mathbf{b} \in \mathbb{R}^d$  is a trainable bias initialized to zero. This tied-weight form makes  $\mathbf{W}^\top \mathbf{W}$  the effective feature-interaction matrix of the model.

**Data.** For each training size  $n$ , we generate sparse random vectors in  $\mathbb{R}^{1000}$ . Each coordinate is independently set to zero with probability 0.99; nonzero entries are sampled uniformly from  $[0, 1)$ , and each vector is then  $\ell_2$ -normalized. We sweep

$$n \in \{3, 5, 8, 10, 15, 30, 50, 100, 200, 500, 1000, 1395, 1946, 2714, 3786, 5282, 7368, 10278, 14337, 20000, 30000, 40000\}. \quad (8)$$

For every  $n$ , the test set size is fixed to 5000, so that changes in  $L_{\text{test}}$  are not caused by changes in test-set variance. The training and test data are generated with deterministic seeds that depend on  $n$ , and we repeat each setting over five model initialization seeds.

**Training.** The model is trained to reconstruct the input using the weighted reconstruction loss

$$\mathcal{L}(\hat{\mathbf{x}}, \mathbf{x}) = \frac{1}{n} \sum_{p=1}^n \sum_{i=1}^d \left( x_i^{(p)} - |\hat{x}_i^{(p)}| \right)^2. \quad (9)$$

All feature-importance weights are set to one. We train for 3000 optimization steps using AdamW with learning rate  $5 \times 10^{-3}$  and weight decay  $10^{-2}$ . The learning-rate schedule consists of a linear warmup over the first 25% of training steps followed by cosine decay. For large training sets, we use mini-batches of size 2048; when  $n < 2048$ , the batch size is clipped to  $n$ . For every training size, we report the mean and standard deviation over five model seeds.

**Evaluation metrics.** For each data size and each model seed, we report the test reconstruction loss  $L_{\text{test}}$  on the fixed test set. We compute the AGOP on the same test distribution, so that interaction metrics are comparable across different training-set sizes.

Because the model uses tied weights, the input AGOP can be computed in closed form without explicitly materializing per-sample Jacobians. Let  $\mathbf{G} = \mathbf{W}^\top \mathbf{W}$  and let

$$\mathbf{m}(\mathbf{x}) = \mathbb{I}[\mathbf{G}\mathbf{x} + \mathbf{b} > 0]$$

be the ReLU activation mask. For this model, averaging  $J_f(\mathbf{x})J_f(\mathbf{x})^\top$  over samples reduces to

$$\mathbf{A} = \mathbf{G}^2 \odot \mathbf{C}, \quad \mathbf{C}_{ij} = \mathbb{E}_{\mathbf{x}} [m_i(\mathbf{x})m_j(\mathbf{x})],$$

where  $\mathbf{C}$  is the empirical co-activation matrix of ReLU gates on the test set. In practice, we accumulate  $\mathbf{C}$  over the test set in chunks and then compute AOFÉ and AOFÉ-ratio from the resulting AGOP matrix  $\mathbf{A}$  using the definitions in the main text. For each training size, the reported curves are the mean over five model seeds, with standard deviations used for error bars. The AGOP heatmaps are obtained by averaging the AGOP matrices across seeds at the selected training sizes.

## B.2 Cross-Network Verification

For CNNs, we use a constant-width residual CNN with a convolutional stem, GroupNorm–GELU residual blocks, global average pooling, and a linear classifier. Models are trained on SVHN after holding out 5,000 validation examples, leaving 68,257 training examples and 26,032 test examples. We fix  $P = 500\text{k}$  and scan depths 2, 3, 4, 6, 8, 10, 12, 14, 16, 20, 24. Training uses AdamW for 60 epochs with learning rate  $7 \times 10^{-4}$ , weight decay 0.05, and batch size 128. AGOP is computed in the input space over all 3072 image coordinates.

For ViTs, we use the same SVHN split and a small vision Transformer with  $4 \times 4$  patches, a class token, learned positional embeddings, pre-norm attention blocks, MLP blocks, and a linear classifier. We fix  $P = 500\text{k}$  and scan depths 1, 2, 3, 4, 6, 8, 12, 14, 16, 20, 24, 26, 30, 36, adjusting the embedding width to match the budget while fixing the attention head dimension to 8. Training uses AdamW for 60 epochs with learning rate  $3 \times 10^{-4}$ , weight decay 0.05, and batch size 128. AGOP is computed at the last transformer block normalization layer and projected to 256 dimensions.

For RNNs, we use a multi-layer GRU classifier on a synthetic temporal interaction task. Each input is a length-32 sequence with 10 channels per step; two marker channels select one position from each half of the sequence, and the label depends on a nonlinear interaction between the marked features plus a weak global temporal context term. We use 20,000 training examples, 10,000 validation examples, and 20,000 test examples. We fix  $P = 50\text{k}$  and scan depths 2, 3, 4, 6, 8, 10, 12, 16, 20, 24, 32. Training uses AdamW for 100 epochs with learning rate  $10^{-3}$ , weight decay 0.01, and batch size 512. AGOP is computed in the flattened input space of dimension 320.

### B.3 Language Models

We evaluate the effect of depth-width shape using decoder-only Transformers trained on byte-level next-token prediction. The task is language modeling on WikiText-103-raw using raw bytes as tokens, with vocabulary size 256 and context length  $T = 256$ . The training objective is per-token cross-entropy in nats.

**Parameter budgets and shape sweep.** We sweep a set of fixed parameter budgets

$$P \in \{0.3\text{M}, 0.6\text{M}, 1.0\text{M}, 1.3\text{M}, 1.6\text{M}, 2.0\text{M}, 2.3\text{M}, 2.7\text{M}, 3.0\text{M}, 5.0\text{M}, 10.0\text{M}\}. \quad (10)$$

For each budget, we scan Transformer depths

$$L \in \{1, 2, 3, 4, 5, 6, 8, 10, 12, 16, 20, 24\}. \quad (11)$$

Given a target budget  $P$  and depth  $L$ , we choose the largest model width  $d_{\text{model}}$  such that the active parameter count does not exceed  $P$ . The width is constrained to be a multiple of the fixed head dimension  $d_{\text{head}} = 4$ , and the number of attention heads is therefore

$$n_{\text{head}} = d_{\text{model}}/d_{\text{head}}. \quad (12)$$

The feed-forward dimension is set to

$$d_{\text{ff}} = 4d_{\text{model}}. \quad (13)$$

We define the depth-width ratio ( $R_{D/W}$ ) as

$$\alpha = \frac{L}{d_{\text{model}}}. \quad (14)$$

Shapes whose parameter padding ratio exceeds 20% are skipped. The reported active parameter count excludes this padding, while the target budget is used to define the fixed-budget sweep.

**Model architecture.** Each model is a decoder-only Transformer with token embeddings, learned positional embeddings, causal self-attention blocks, MLP blocks, residual connections, and layer normalization. The language modeling head maps the final hidden state to 256 byte logits. Dropout is set to zero. Linear and embedding weights are initialized from a normal distribution with standard deviation 0.02, with residual projection weights scaled by the depth-dependent GPT-style factor.

**Training data and optimization.** For a target parameter budget  $P$ , the byte-level training budget is

$$D = 60P \quad (15)$$

bytes. This corresponds approximately to a Chinchilla-style budget of  $20P$  BPE tokens under the rough conversion of three bytes per BPE token. Training examples are random windows of length 256 sampled from the WikiText-103 training split. Validation and test losses are evaluated using deterministic non-overlapping windows from the validation and test splits.

Models are trained with AdamW using learning rate  $3 \times 10^{-4}$ , weight decay  $10^{-2}$ , batch size 64, and gradient clipping at norm 1.0. The learning rate follows a linear warmup for 300 steps followed by cosine decay. Let

$$S_0 = \max\left(200, \left\lfloor \frac{D/256}{64} \right\rfloor\right) \quad (16)$$

be the base number of training steps. Training is allowed to continue up to  $1.5S_0$  steps, with early stopping based on validation cross-entropy after the base budget has been reached. Validation is checked every 200 steps, and the best validation checkpoint is restored before final evaluation.

**Evaluation metrics.** The primary performance metric is test cross-entropy  $L_{\text{test}}$ , reported in nats per byte on the held-out WikiText-103 test split. After training, we restore the checkpoint with the best validation cross-entropy and evaluate train, validation, and test cross-entropy.

For the interaction metrics, we estimate a fixed-size projected AGOP so that AGOP matrices are comparable across Transformer widths. For each input window, we take the last-position logits  $\ell_T(\mathbf{x}) \in \mathbb{R}^{256}$  and project them with a fixed Gaussian matrix  $\mathbf{P} \in \mathbb{R}^{64 \times 256}$  shared across all budgets and shapes. This gives projected logits

$$\mathbf{z}_T(\mathbf{x}) = \mathbf{P}\ell_T(\mathbf{x}) \in \mathbb{R}^{64}.$$

We then estimate the AGOP of  $\mathbf{z}_T$  with respect to the input embedding sequence. Rather than forming the full Jacobian explicitly, we use random Jacobian-vector products: for Gaussian tangent vectors  $\mathbf{u}$ ,

$$\mathbb{E}_{\mathbf{u}} [(J_P \mathbf{u})(J_P \mathbf{u})^\top] = J_P J_P^\top.$$

Thus each JVP contributes one rank-one estimate of the projected AGOP. In our experiments, the estimate uses 4 randomly sampled data batches, batch size 128, and 64 JVP samples per batch. The resulting  $64 \times 64$  AGOP is symmetrized, and AOFE and AOFE-ratio are computed from this matrix using the definitions in the main text.

## C Experiment Results

### C.1 Double Descent

Table 1: Double Descent Experimental Results

data_size	test_loss_mean	AOFE-ratio	AOFE
3	1.1026	0.8191	5.7744e+00
5	0.9989	0.1531	2.7222e-01
8	1.0077	0.5436	3.7300e-02
10	1.0073	0.7388	2.2145e-01
15	1.0036	0.5865	4.3480e-02
30	1.0103	0.8132	1.0139e+01
50	1.0093	0.8189	1.0006e+01
100	1.0321	0.9197	3.4957e+02
200	1.2483	0.9469	3.2721e+04
500	1.5340	0.9544	1.1586e+05
1000	1.0583	0.7598	7.3324e+02
1395	1.0000	0.7426	1.1109e+01
1946	0.9945	0.9175	2.1968e+00
2714	0.9932	0.9266	1.5502e+00
3786	0.9932	0.9473	1.8220e+00
5282	0.9927	0.9395	1.6790e+00
7368	0.9933	0.9221	1.4221e+00
10278	0.9930	0.9106	1.3514e+00
14337	0.9931	0.9060	1.4063e+00
20000	0.9931	0.8933	1.2267e+00
30000	0.9936	0.8871	1.3895e+00
40000	0.9932	0.8787	1.4859e+00

### C.2 Cross Network Verification

Table 2: Depth-width sweep results for the CNN on SVHN at a fixed 500K parameter budget.

$P_{target}$	$D$	$W$	$R_{D/W}$	AOFE	$L_{train}$	$L_{val}$	$L_{test}$	$R_{AOFE}$
500000	2	120	0.0167	0.6387	0.0589	0.3613	0.2850	0.7634
500000	3	96	0.0312	0.4873	0.0042	0.3287	0.2482	0.7967
500000	4	80	0.0500	0.5629	0.0009	0.3358	0.2642	0.8227
500000	6	64	0.0938	0.8052	0.0011	0.3040	0.2568	0.8418
500000	8	56	0.1429	0.9423	0.0030	0.2919	0.2449	0.8732
500000	10	56	0.1786	1.0195	0.0039	0.2806	0.2527	0.8856
500000	12	48	0.2500	1.9773	0.0090	0.2924	0.2296	0.9209
500000	14	48	0.2917	1.5752	0.0088	0.2751	0.2193	0.9174
500000	16	40	0.4000	1.7485	0.0090	0.2755	0.2355	0.9050
500000	20	40	0.5000	2.6821	0.0116	0.2794	0.2249	0.9268
500000	24	32	0.7500	3.5590	0.0134	0.2888	0.2299	0.9261

Table 3: Depth-width sweep results for the GRU on the temporal-interaction task at a fixed 50K parameter budget.

$P_{target}$	$D$	$W$	$R_{D/W}$	AOFE	$L_{train}$	$L_{val}$	$L_{test}$	$R_{AOFE}$
50000	2	72	0.0278	115.9646	0.1013	0.1773	0.1686	0.6478
50000	3	56	0.0536	186.5604	0.1006	0.1662	0.1596	0.5524
50000	4	48	0.0833	27.6484	0.1047	0.1528	0.1502	0.6350
50000	6	40	0.1500	48.5346	0.0966	0.1444	0.1420	0.7397
50000	8	32	0.2500	508.7877	0.1082	0.1514	0.1402	0.8447
50000	10	32	0.3125	55.0359	0.0883	0.1467	0.1428	0.7263
50000	12	24	0.5000	84.0977	0.1075	0.1498	0.1499	0.7191
50000	16	24	0.6667	101.1637	0.1043	0.1439	0.1441	0.7180
50000	20	16	1.2500	58.0671	0.1058	0.1485	0.1395	0.7119
50000	24	16	1.5000	21.4883	0.1174	0.1506	0.1438	0.6898
50000	32	16	2.0000	63.1332	0.2988	0.3350	0.1598	0.6371

Table 4: Depth-width sweep results for the Vision Transformer on SVHN at a fixed 500K parameter budget.

$P_{target}$	$D$	$W$	$R_{D/W}$	AOFE	$L_{train}$	$L_{val}$	$L_{test}$	$R_{AOFE}$
500000	1	200	0.0050	0.0001	0.0001	0.9619	1.0401	0.5029
500000	2	144	0.0139	0.0000	0.0001	0.8919	0.9611	0.6880
500000	3	112	0.0268	0.0000	0.0014	0.8979	1.0171	0.7835
500000	4	104	0.0385	0.0000	0.0002	0.7398	0.8181	0.7865
500000	6	80	0.0750	0.0000	0.0059	0.8233	0.9277	0.8474
500000	8	72	0.1111	0.0000	0.0059	0.7901	0.8674	0.8301
500000	12	56	0.2143	0.0000	0.0150	0.6895	0.7751	0.8866
500000	14	56	0.2500	0.0000	0.0054	0.7015	0.7394	0.8584
500000	16	48	0.3333	0.0000	0.0104	0.6427	0.7093	0.9202
500000	20	48	0.4167	0.0000	0.0141	0.6648	0.7501	0.8925
500000	24	40	0.6000	0.0000	0.0183	0.6022	0.6674	0.9395
500000	26	40	0.6500	0.0000	0.0258	0.6400	0.6792	0.9744
500000	30	40	0.7500	0.0001	0.0119	0.6554	0.6929	0.9518
500000	36	32	1.1250	0.0001	0.0562	0.5219	0.5398	0.9850

### C.3 Language Models

Table 5: Model Configurations for Parameter Budgets Ranging from 0.3M to 1.3M

ID	target_N	depth	d_model	n_heads	d_ff	active_N	depth_width_ratio
0.3M-1	300000	1	128	32	512	295680	0.0078
0.3M-2	300000	2	96	24	384	295872	0.0208
0.3M-3	300000	3	80	20	320	292960	0.0375
0.3M-4	300000	4	68	17	272	275400	0.0588
0.3M-5	300000	5	64	16	256	296320	0.0781
0.3M-6	300000	6	56	14	224	270256	0.1071
0.3M-8	300000	8	48	12	192	259680	0.1667
0.3M-10	300000	10	44	11	176	267960	0.2273
0.3M-12	300000	12	40	10	160	263120	0.3000
0.3M-16	300000	16	36	9	144	278856	0.4444
0.3M-20	300000	20	32	8	128	272960	0.6250
0.3M-24	300000	24	28	7	112	250040	0.8571
0.6M-1	600000	1	192	48	768	590976	0.0052
0.6M-2	600000	2	140	35	560	579320	0.0143
0.6M-3	600000	3	116	29	464	575128	0.0259
0.6M-4	600000	4	100	25	400	558600	0.0400
0.6M-5	600000	5	92	23	368	580520	0.0543
0.6M-6	600000	6	84	21	336	574728	0.0714
0.6M-8	600000	8	72	18	288	555408	0.1111
0.6M-10	600000	10	64	16	256	543360	0.1562
0.6M-12	600000	12	60	15	240	567480	0.2000
0.6M-16	600000	16	52	13	208	562536	0.3077
0.6M-20	600000	20	48	12	192	593760	0.4167
0.6M-24	600000	24	44	11	176	595672	0.5455
1M-1	1000000	1	256	64	1024	984576	0.0039
1M-2	1000000	2	188	47	752	994520	0.0106
1M-3	1000000	3	156	39	624	998088	0.0192
1M-4	1000000	4	136	34	544	994704	0.0294
1M-5	1000000	5	120	30	480	958800	0.0417
1M-6	1000000	6	112	28	448	992096	0.0536
1M-8	1000000	8	96	24	384	961728	0.0833
1M-10	1000000	10	84	21	336	914760	0.1190
1M-12	1000000	12	80	20	320	987040	0.1500
1M-16	1000000	16	68	17	272	944520	0.2353
1M-20	1000000	20	60	15	240	915000	0.3333
1M-24	1000000	24	56	14	224	951664	0.4286
1.3M-1	1300000	1	296	74	1184	1280496	0.0034
1.3M-2	1300000	2	216	54	864	1287792	0.0093
1.3M-3	1300000	3	176	44	704	1252768	0.0170
1.3M-4	1300000	4	156	39	624	1290744	0.0256
1.3M-5	1300000	5	140	35	560	1286600	0.0357
1.3M-6	1300000	6	128	32	512	1281280	0.0469
1.3M-8	1300000	8	112	28	448	1294048	0.0714
1.3M-10	1300000	10	100	25	400	1281000	0.1000
1.3M-12	1300000	12	92	23	368	1294072	0.1304
1.3M-16	1300000	16	80	20	320	1295520	0.2000
1.3M-20	1300000	20	68	17	272	1167560	0.2941
1.3M-24	1300000	24	64	16	256	1235072	0.3750

Table 6: Training Metrics for Parameter Budgets Ranging from 0.3M to 1.3M

ID	train_loss	val_loss	test_loss	AOFE	AOFE-ratio
0.3M-1	2.2141	2.2108	2.2186	1.45e+11	0.6311
0.3M-2	2.2289	2.2282	2.2353	8.59e+10	0.6298
0.3M-3	2.2404	2.2399	2.2472	1.24e+11	0.6488
0.3M-4	2.2677	2.2674	2.2729	6.55e+10	0.5993
0.3M-5	2.2529	2.2520	2.2566	1.01e+11	0.6048
0.3M-6	2.2800	2.2789	2.2851	8.16e+10	0.5717
0.3M-8	2.3433	2.3437	2.3490	9.54e+10	0.5625
0.3M-10	2.3199	2.3191	2.3245	4.73e+10	0.5299
0.3M-12	2.3912	2.3929	2.3979	2.56e+10	0.5317
0.3M-16	2.3973	2.3975	2.4035	2.93e+10	0.5539
0.3M-20	2.4333	2.4339	2.4383	2.75e+10	0.5456
0.3M-24	2.4779	2.4786	2.4830	1.89e+10	0.4554
0.6M-1	1.8316	1.8186	1.8375	2.10e+10	0.7253
0.6M-2	1.8110	1.8016	1.8154	1.69e+11	0.7266
0.6M-3	1.7776	1.7654	1.7839	3.98e+11	0.7379
0.6M-4	1.7420	1.7294	1.7461	2.40e+11	0.7386
0.6M-5	1.7410	1.7282	1.7450	2.45e+11	0.6856
0.6M-6	1.7293	1.7154	1.7342	1.40e+11	0.6857
0.6M-8	1.7868	1.7744	1.7913	1.71e+11	0.6582
0.6M-10	1.7925	1.7793	1.7971	2.57e+11	0.6586
0.6M-12	1.8462	1.8358	1.8519	1.22e+11	0.6381
0.6M-16	1.9109	1.9029	1.9172	1.67e+11	0.6206
0.6M-20	1.9142	1.9053	1.9206	1.40e+11	0.5469
0.6M-24	1.9732	1.9649	1.9776	1.59e+11	0.5551
1M-1	1.5650	1.5451	1.5680	3.84e+11	0.7680
1M-2	1.5447	1.5260	1.5480	3.82e+11	0.7738
1M-3	1.4478	1.4285	1.4514	2.48e+11	0.7658
1M-4	1.4444	1.4244	1.4459	1.39e+11	0.7786
1M-5	1.4433	1.4220	1.4459	1.34e+11	0.7649
1M-6	1.4565	1.4348	1.4616	7.71e+10	0.7803
1M-8	1.4600	1.4400	1.4635	1.03e+11	0.7419
1M-10	1.4993	1.4791	1.5005	6.73e+10	0.7233
1M-12	1.4889	1.4678	1.4890	7.43e+10	0.7097
1M-16	1.5442	1.5256	1.5458	6.27e+10	0.6960
1M-20	1.6046	1.5870	1.6081	8.30e+10	0.6681
1M-24	1.6217	1.6046	1.6241	7.59e+10	0.6396
1.3M-1	1.4772	1.4571	1.4793	4.82e+09	0.7858
1.3M-2	1.4570	1.4363	1.4607	2.74e+11	0.8209
1.3M-3	1.3689	1.3485	1.3723	2.07e+11	0.8123
1.3M-4	1.3667	1.3468	1.3683	1.04e+11	0.8079
1.3M-5	1.3494	1.3298	1.3517	9.12e+10	0.8096
1.3M-6	1.3453	1.3249	1.3487	6.96e+10	0.7899
1.3M-8	1.3613	1.3412	1.3625	6.72e+10	0.8007
1.3M-10	1.3696	1.3495	1.3703	3.82e+10	0.7716
1.3M-12	1.3845	1.3625	1.3871	4.14e+10	0.7721
1.3M-16	1.4149	1.3940	1.4161	3.73e+10	0.7316
1.3M-20	1.4487	1.4274	1.4499	4.98e+10	0.7424
1.3M-24	1.4611	1.4396	1.4615	4.18e+10	0.7111

Table 7: Model Configurations for Parameter Budgets Ranging from 1.6M to 2.7M

ID	target_N	depth	d_model	n_heads	d_ff	active_N	depth_width_ratio
1.6M-1	1600000	1	332	83	1328	1579656	0.0030
1.6M-2	1600000	2	240	60	960	1569120	0.0083
1.6M-3	1600000	3	200	50	800	1596400	0.0150
1.6M-4	1600000	4	172	43	688	1555224	0.0233
1.6M-5	1600000	5	156	39	624	1583400	0.0321
1.6M-6	1600000	6	140	35	560	1522360	0.0429
1.6M-8	1600000	8	124	31	496	1575544	0.0645
1.6M-10	1600000	10	112	28	448	1596000	0.0893
1.6M-12	1600000	12	100	25	400	1521800	0.1200
1.6M-16	1600000	16	88	22	352	1560240	0.1818
1.6M-20	1600000	20	76	19	304	1450840	0.2632
1.6M-24	1600000	24	72	18	288	1555344	0.3333
2M-1	2000000	1	376	94	1504	1987536	0.0027
2M-2	2000000	2	272	68	1088	1987232	0.0074
2M-3	2000000	3	224	56	896	1981504	0.0134
2M-4	2000000	4	196	49	784	1998024	0.0204
2M-5	2000000	5	176	44	704	1997600	0.0284
2M-6	2000000	6	160	40	640	1970240	0.0375
2M-8	2000000	8	140	35	560	1993880	0.0571
2M-10	2000000	10	124	31	496	1945560	0.0806
2M-12	2000000	12	112	28	448	1897952	0.1071
2M-16	2000000	16	96	24	384	1849536	0.1667
2M-20	2000000	20	88	22	352	1933360	0.2273
2M-24	2000000	24	80	20	320	1912480	0.3000
2.3M-1	2300000	1	404	101	1616	2271288	0.0025
2.3M-2	2300000	2	292	73	1168	2273512	0.0068
2.3M-3	2300000	3	240	60	960	2261280	0.0125
2.3M-4	2300000	4	208	52	832	2240160	0.0192
2.3M-5	2300000	5	188	47	752	2269160	0.0266
2.3M-6	2300000	6	172	43	688	2266616	0.0349
2.3M-8	2300000	8	148	37	592	2221480	0.0541
2.3M-10	2300000	10	132	33	528	2197800	0.0758
2.3M-12	2300000	12	120	30	480	2171760	0.1000
2.3M-16	2300000	16	104	26	416	2163408	0.1538
2.3M-20	2300000	20	96	24	384	2293440	0.2083
2.3M-24	2300000	24	84	21	336	2104872	0.2857
2.7M-1	2700000	1	440	110	1760	2663760	0.0023
2.7M-2	2700000	2	316	79	1264	2642392	0.0063
2.7M-3	2700000	3	260	65	1040	2636920	0.0115
2.7M-4	2700000	4	228	57	912	2674440	0.0175
2.7M-5	2700000	5	204	51	816	2658120	0.0245
2.7M-6	2700000	6	188	47	752	2694040	0.0319
2.7M-8	2700000	8	160	40	640	2585920	0.0500
2.7M-10	2700000	10	144	36	576	2604960	0.0694
2.7M-12	2700000	12	132	33	528	2617032	0.0909
2.7M-16	2700000	16	116	29	464	2680296	0.1379
2.7M-20	2700000	20	104	26	416	2684240	0.1923
2.7M-24	2700000	24	92	23	368	2517304	0.2609

Table 8: Training Metrics for Parameter Budgets Ranging from 1.6M to 2.7M

ID	train_loss	val_loss	test_loss	AOFE	AOFE-ratio
1.6M-1	1.4067	1.3879	1.4094	5.98e+10	0.8138
1.6M-2	1.3869	1.3659	1.3891	2.92e+11	0.8400
1.6M-3	1.3102	1.2900	1.3150	1.54e+11	0.8522
1.6M-4	1.3046	1.2855	1.3077	1.05e+11	0.8400
1.6M-5	1.2863	1.2679	1.2909	6.44e+10	0.8427
1.6M-6	1.2953	1.2769	1.2996	5.90e+10	0.8325
1.6M-8	1.2997	1.2809	1.3028	3.08e+10	0.8246
1.6M-10	1.3175	1.2967	1.3209	4.33e+10	0.8267
1.6M-12	1.3219	1.3017	1.3240	3.27e+10	0.7900
1.6M-16	1.3388	1.3183	1.3418	3.85e+10	0.7703
1.6M-20	1.3633	1.3418	1.3638	3.43e+10	0.7424
1.6M-24	1.3852	1.3646	1.3863	4.87e+10	0.7363
2M-1	1.3717	1.3530	1.3755	2.94e+11	0.8304
2M-2	1.3508	1.3295	1.3518	2.70e+11	0.8771
2M-3	1.2561	1.2391	1.2623	1.03e+11	0.8632
2M-4	1.2488	1.2320	1.2534	6.29e+10	0.8678
2M-5	1.2293	1.2120	1.2340	5.03e+10	0.8477
2M-6	1.2525	1.2349	1.2566	3.45e+10	0.8506
2M-8	1.2482	1.2302	1.2518	3.28e+10	0.8363
2M-10	1.2531	1.2344	1.2568	3.34e+10	0.8286
2M-12	1.2691	1.2510	1.2730	2.69e+10	0.8278
2M-16	1.2802	1.2614	1.2820	3.02e+10	0.8099
2M-20	1.2874	1.2675	1.2898	2.10e+10	0.7861
2M-24	1.3132	1.2922	1.3143	2.64e+10	0.7662
2.3M-1	1.3505	1.3313	1.3538	1.86e+10	0.8440
2.3M-2	1.3259	1.3053	1.3293	2.05e+11	0.8868
2.3M-3	1.2349	1.2181	1.2377	8.03e+10	0.8861
2.3M-4	1.2248	1.2089	1.2267	4.68e+10	0.8715
2.3M-5	1.2160	1.1990	1.2206	2.95e+10	0.8652
2.3M-6	1.2111	1.1947	1.2138	3.07e+10	0.8678
2.3M-8	1.2141	1.1978	1.2180	2.52e+10	0.8493
2.3M-10	1.2299	1.2130	1.2330	2.31e+10	0.8475
2.3M-12	1.2446	1.2260	1.2463	2.27e+10	0.8399
2.3M-16	1.2505	1.2325	1.2556	1.62e+10	0.8236
2.3M-20	1.2504	1.2314	1.2527	1.88e+10	0.8150
2.3M-24	1.2707	1.2507	1.2717	1.88e+10	0.7912
2.7M-1	1.3071	1.2904	1.3128	2.50e+12	0.8590
2.7M-2	1.3034	1.2843	1.3043	1.47e+11	0.9007
2.7M-3	1.2014	1.1858	1.2067	5.25e+10	0.8961
2.7M-4	1.1890	1.1732	1.1944	3.23e+10	0.8767
2.7M-5	1.1783	1.1631	1.1847	3.13e+10	0.8810
2.7M-6	1.1857	1.1694	1.1897	2.49e+10	0.8749
2.7M-8	1.1881	1.1707	1.1931	1.69e+10	0.8767
2.7M-10	1.1872	1.1706	1.1904	1.49e+10	0.8648
2.7M-12	1.1924	1.1762	1.1955	1.80e+10	0.8501
2.7M-16	1.2017	1.1853	1.2057	1.73e+10	0.8465
2.7M-20	1.2126	1.1964	1.2154	1.38e+10	0.8258
2.7M-24	1.2274	1.2079	1.2293	1.40e+10	0.8173

Table 9: Model Configurations for Parameter Budgets Ranging from 3.0M to 10.0M

ID	target_N	depth	d_model	n_heads	d_ff	active_N	depth_width_ratio
3M-1	3000000	1	468	117	1872	2990520	0.0021
3M-2	3000000	2	336	84	1344	2970912	0.0060
3M-3	3000000	3	276	69	1104	2958168	0.0109
3M-4	3000000	4	240	60	960	2953440	0.0167
3M-5	3000000	5	216	54	864	2970000	0.0231
3M-6	3000000	6	196	49	784	2921576	0.0306
3M-8	3000000	8	172	43	688	2978008	0.0465
3M-10	3000000	10	152	38	608	2895600	0.0658
3M-12	3000000	12	140	35	560	2936920	0.0857
3M-16	3000000	16	120	30	480	2864880	0.1333
3M-20	3000000	20	108	27	432	2891160	0.1852
3M-24	3000000	24	100	25	400	2966600	0.2400
5M-1	5000000	1	612	153	2448	4968216	0.0016
5M-2	5000000	2	440	110	1760	4988720	0.0045
5M-3	5000000	3	360	90	1440	4947120	0.0083
5M-4	5000000	4	312	78	1248	4917744	0.0128
5M-5	5000000	5	280	70	1120	4925200	0.0179
5M-6	5000000	6	256	64	1024	4921856	0.0234
5M-8	5000000	8	224	56	896	4996544	0.0357
5M-10	5000000	10	200	50	800	4962000	0.0500
5M-12	5000000	12	180	45	720	4812840	0.0667
10M-4	10000000	4	448	112	1792	9985920	0.0089
10M-5	10000000	5	400	100	1600	9916000	0.0125
10M-6	10000000	6	364	91	1456	9828728	0.0165
10M-8	10000000	8	316	79	1264	9839608	0.0253
10M-10	10000000	10	284	71	1136	9908760	0.0352
10M-12	10000000	12	256	64	1024	9487424	0.0469
10M-14	10000000	14	240	60	960	9875040	0.0583

Table 10: Training Metrics for Parameter Budgets Ranging from 3.0M to 10.0M

ID	train_loss	val_loss	test_loss	AOFE	AOFE-ratio
3M-1	1.2977	1.2807	1.3020	9.03e+10	0.8736
3M-2	1.2780	1.2600	1.2817	1.93e+11	0.9003
3M-3	1.1831	1.1671	1.1885	3.96e+10	0.8916
3M-4	1.1701	1.1541	1.1743	2.47e+10	0.8900
3M-5	1.1554	1.1398	1.1598	2.48e+10	0.8947
3M-6	1.1622	1.1457	1.1675	2.18e+10	0.8846
3M-8	1.1610	1.1458	1.1660	2.06e+10	0.8786
3M-10	1.1625	1.1472	1.1661	1.26e+10	0.8721
3M-12	1.1690	1.1534	1.1727	1.77e+10	0.8613
3M-16	1.1780	1.1619	1.1823	1.18e+10	0.8407
3M-20	1.1927	1.1752	1.1948	1.11e+10	0.8356
3M-24	1.1933	1.1767	1.1968	1.14e+10	0.8246
5M-1	1.2360	1.2209	1.2397	1.06e+11	0.9024
5M-2	1.1981	1.1826	1.2032	9.32e+10	0.9178
5M-3	1.0995	1.0864	1.1062	1.18e+10	0.9234
5M-4	1.0905	1.0777	1.0967	4.19e+09	0.9219
5M-5	1.0727	1.0615	1.0783	7.79e+09	0.9184
5M-6	1.0781	1.0656	1.0836	7.86e+09	0.9113
5M-8	1.0733	1.0603	1.0777	4.93e+09	0.9043
5M-10	1.0731	1.0600	1.0786	7.46e+09	0.9046
5M-12	1.0782	1.0656	1.0825	6.37e+09	0.8980
10M-4	0.9871	0.9816	0.9979	1.42e+09	0.9446
10M-5	0.9751	0.9699	0.9862	1.25e+09	0.9360
10M-6	0.9676	0.9635	0.9790	9.69e+08	0.9355
10M-8	0.9665	0.9627	0.9774	7.45e+08	0.9294
10M-10	0.9625	0.9584	0.9732	5.90e+08	0.9227
10M-12	NaN	NaN	NaN	5.30e-02	NaN
10M-14	0.9652	0.9603	0.9761	4.48e+08	0.9204

## D Configuration Details for Models Included in the Comparison in Figure 4

Table 11: Configuration Details for Models in Comparison in Figure 4

model	family	params_B	d_model	layers	mmlu_pro	param_group	alpha	distance_to_interval	vertical_layer_gap
Qwen2.5-0.5B	Qwen2.5	0.5000	896	24	10.0600	0.5-1B	0.0268	0.0000	0.0000
Llama-3.2-1B-Inst	Llama	1.2300	2048	16	7.5800	0.5-1B	0.0078	0.0152	31.1040
Gemma-3-1B-IT	Gemma	1.0000	1152	26	13.5000	0.5-1B	0.0226	0.0004	0.4960
Qwen2.5-1.5B	Qwen2.5	1.5000	1536	28	20.6100	1-2.5B	0.0182	0.0048	7.3280
Qwen3-1.7B	Qwen3	1.7000	2048	28	19.8000	1-2.5B	0.0137	0.0093	19.1040
SmolLM2-1.7B	SmolLM	1.7000	2048	24	12.6400	1-2.5B	0.0117	0.0113	23.1040
Gemma-2-2B	Gemma	2.0000	2304	26	13.5200	1-2.5B	0.0113	0.0117	26.9920
Qwen2.5-3B-Inst	Qwen2.5	3.4000	2048	36	25.0500	3-4.5B	0.0176	0.0054	11.1040
Llama-3.2-3B-Inst	Llama	3.2100	3072	28	24.3900	3-4.5B	0.0091	0.0139	42.6560
Phi-3.5-mini	Phi	3.8000	3072	32	32.9100	3-4.5B	0.0104	0.0126	38.6560
MiniCPM3-4B	MiniCPM	4.0000	2560	62	43.0000	3-4.5B	0.0242	0.0000	0.0000
Gemma-3-4B-PT	Gemma	4.0000	2560	34	29.2000	3-4.5B	0.0133	0.0097	24.8800
Qwen3-4B	Qwen3	4.0000	2560	36	48.0000	3-4.5B	0.0141	0.0089	22.8800
Mistral-7B-Inst-v0.3	Mistral	7.2500	4096	32	23.0600	7-9B	0.0078	0.0152	62.2080
Falcon3-7B-Inst	Falcon	7.4600	3072	28	34.3000	7-9B	0.0091	0.0139	42.6560
Qwen2.5-7B-Inst	Qwen2.5	7.6000	3584	28	36.5200	7-9B	0.0078	0.0152	54.4320
Llama-3.1-8B-Inst	Llama	8.0000	4096	32	30.6800	7-9B	0.0078	0.0152	62.2080
Gemma-2-9B-IT	Gemma	9.0000	3584	42	31.9500	7-9B	0.0117	0.0113	40.4320

## E Limitations

Unlike the TinyGPT sweep, the compared models were not trained under a common tokenizer, dataset, compute budget, optimizer, context length, or post-training protocol. MMLU-Pro is also sensitive to instruction tuning, synthetic reasoning data, prompt format, and reasoning-style evaluation, all of which can alter scores without changing base architecture. Restricting to dense small models improves comparability but limits scope, and the numerical interval (0.023–0.047) was obtained from a byte-level TinyGPT setting rather than billion-scale LLM training. We therefore do not claim universality of the interval nor that distance to it alone explains LLM performance. The more conservative conclusion is that the observed negative trends provide external, non-controlled evidence for the paper’s main mechanism: under fixed budget and architecture class, depth-width shape can regulate interaction efficiency, and interaction efficiency is associated with generalization.

## NeurIPS Paper Checklist

### 1. Claims

Question: Do the main claims made in the abstract and introduction accurately reflect the paper’s contributions and scope?

Answer: [Yes].

Justification: The claims match theoretical and experimental results.

Guidelines:

- The answer [N/A] means that the abstract and introduction do not include the claims made in the paper.
- The abstract and/or introduction should clearly state the claims made, including the contributions made in the paper and important assumptions and limitations. A [No] or [N/A] answer to this question will not be perceived well by the reviewers.
- The claims made should match theoretical and experimental results, and reflect how much the results can be expected to generalize to other settings.
- It is fine to include aspirational goals as motivation as long as it is clear that these goals are not attained by the paper.

### 2. Limitations

Question: Does the paper discuss the limitations of the work performed by the authors?

Answer: [Yes].

Justification: We include the limitations in the Discussion section and also in the Appendices.

Guidelines:

- The answer [N/A] means that the paper has no limitation while the answer [No] means that the paper has limitations, but those are not discussed in the paper.
- The authors are encouraged to create a separate “Limitations” section in their paper.
- The paper should point out any strong assumptions and how robust the results are to violations of these assumptions (e.g., independence assumptions, noiseless settings, model well-specification, asymptotic approximations only holding locally). The authors should reflect on how these assumptions might be violated in practice and what the implications would be.
- The authors should reflect on the scope of the claims made, e.g., if the approach was only tested on a few datasets or with a few runs. In general, empirical results often depend on implicit assumptions, which should be articulated.
- The authors should reflect on the factors that influence the performance of the approach. For example, a facial recognition algorithm may perform poorly when image resolution is low or images are taken in low lighting. Or a speech-to-text system might not be used reliably to provide closed captions for online lectures because it fails to handle technical jargon.
- The authors should discuss the computational efficiency of the proposed algorithms and how they scale with dataset size.
- If applicable, the authors should discuss possible limitations of their approach to address problems of privacy and fairness.
- While the authors might fear that complete honesty about limitations might be used by reviewers as grounds for rejection, a worse outcome might be that reviewers discover limitations that aren’t acknowledged in the paper. The authors should use their best judgment and recognize that individual actions in favor of transparency play an important role in developing norms that preserve the integrity of the community. Reviewers will be specifically instructed to not penalize honesty concerning limitations.

### 3. Theory assumptions and proofs

Question: For each theoretical result, does the paper provide the full set of assumptions and a complete (and correct) proof?

Answer: [Yes].

Justification: All assumptions are clearly stated.

Guidelines:

- The answer [N/A] means that the paper does not include theoretical results.
- All the theorems, formulas, and proofs in the paper should be numbered and cross-referenced.
- All assumptions should be clearly stated or referenced in the statement of any theorems.
- The proofs can either appear in the main paper or the supplemental material, but if they appear in the supplemental material, the authors are encouraged to provide a short proof sketch to provide intuition.
- Inversely, any informal proof provided in the core of the paper should be complemented by formal proofs provided in appendix or supplemental material.
- Theorems and Lemmas that the proof relies upon should be properly referenced.

#### 4. Experimental result reproducibility

Question: Does the paper fully disclose all the information needed to reproduce the main experimental results of the paper to the extent that it affects the main claims and/or conclusions of the paper (regardless of whether the code and data are provided or not)?

Answer: [Yes].

Justification: We provide all details to reproduce.

Guidelines:

- The answer [N/A] means that the paper does not include experiments.
- If the paper includes experiments, a [No] answer to this question will not be perceived well by the reviewers: Making the paper reproducible is important, regardless of whether the code and data are provided or not.
- If the contribution is a dataset and/or model, the authors should describe the steps taken to make their results reproducible or verifiable.
- Depending on the contribution, reproducibility can be accomplished in various ways. For example, if the contribution is a novel architecture, describing the architecture fully might suffice, or if the contribution is a specific model and empirical evaluation, it may be necessary to either make it possible for others to replicate the model with the same dataset, or provide access to the model. In general, releasing code and data is often one good way to accomplish this, but reproducibility can also be provided via detailed instructions for how to replicate the results, access to a hosted model (e.g., in the case of a large language model), releasing of a model checkpoint, or other means that are appropriate to the research performed.
- While NeurIPS does not require releasing code, the conference does require all submissions to provide some reasonable avenue for reproducibility, which may depend on the nature of the contribution. For example
  - (a) If the contribution is primarily a new algorithm, the paper should make it clear how to reproduce that algorithm.
  - (b) If the contribution is primarily a new model architecture, the paper should describe the architecture clearly and fully.
  - (c) If the contribution is a new model (e.g., a large language model), then there should either be a way to access this model for reproducing the results or a way to reproduce the model (e.g., with an open-source dataset or instructions for how to construct the dataset).
  - (d) We recognize that reproducibility may be tricky in some cases, in which case authors are welcome to describe the particular way they provide for reproducibility. In the case of closed-source models, it may be that access to the model is limited in some way (e.g., to registered users), but it should be possible for other researchers to have some path to reproducing or verifying the results.

#### 5. Open access to data and code

Question: Does the paper provide open access to the data and code, with sufficient instructions to faithfully reproduce the main experimental results, as described in supplemental material?

Answer: [Yes].

Justification: We submit our code in the supplementary material.

Guidelines:

- The answer [N/A] means that paper does not include experiments requiring code.
- Please see the NeurIPS code and data submission guidelines (<https://neurips.cc/public/guides/CodeSubmissionPolicy>) for more details.
- While we encourage the release of code and data, we understand that this might not be possible, so [No] is an acceptable answer. Papers cannot be rejected simply for not including code, unless this is central to the contribution (e.g., for a new open-source benchmark).
- The instructions should contain the exact command and environment needed to run to reproduce the results. See the NeurIPS code and data submission guidelines (<https://neurips.cc/public/guides/CodeSubmissionPolicy>) for more details.
- The authors should provide instructions on data access and preparation, including how to access the raw data, preprocessed data, intermediate data, and generated data, etc.
- The authors should provide scripts to reproduce all experimental results for the new proposed method and baselines. If only a subset of experiments are reproducible, they should state which ones are omitted from the script and why.
- At submission time, to preserve anonymity, the authors should release anonymized versions (if applicable).
- Providing as much information as possible in supplemental material (appended to the paper) is recommended, but including URLs to data and code is permitted.

## 6. Experimental setting/details

Question: Does the paper specify all the training and test details (e.g., data splits, hyperparameters, how they were chosen, type of optimizer) necessary to understand the results?

Answer: [Yes].

Justification: We explained these details in our Appendices.

Guidelines:

- The answer [N/A] means that the paper does not include experiments.
- The experimental setting should be presented in the core of the paper to a level of detail that is necessary to appreciate the results and make sense of them.
- The full details can be provided either with the code, in appendix, or as supplemental material.

## 7. Experiment statistical significance

Question: Does the paper report error bars suitably and correctly defined or other appropriate information about the statistical significance of the experiments?

Answer: [Yes].

Justification: We included error bars.

Guidelines:

- The answer [N/A] means that the paper does not include experiments.
- The authors should answer [Yes] if the results are accompanied by error bars, confidence intervals, or statistical significance tests, at least for the experiments that support the main claims of the paper.
- The factors of variability that the error bars are capturing should be clearly stated (for example, train/test split, initialization, random drawing of some parameter, or overall run with given experimental conditions).
- The method for calculating the error bars should be explained (closed form formula, call to a library function, bootstrap, etc.)
- The assumptions made should be given (e.g., Normally distributed errors).
- It should be clear whether the error bar is the standard deviation or the standard error of the mean.

- It is OK to report 1-sigma error bars, but one should state it. The authors should preferably report a 2-sigma error bar than state that they have a 96% CI, if the hypothesis of Normality of errors is not verified.
- For asymmetric distributions, the authors should be careful not to show in tables or figures symmetric error bars that would yield results that are out of range (e.g., negative error rates).
- If error bars are reported in tables or plots, the authors should explain in the text how they were calculated and reference the corresponding figures or tables in the text.

#### 8. Experiments compute resources

Question: For each experiment, does the paper provide sufficient information on the computer resources (type of compute workers, memory, time of execution) needed to reproduce the experiments?

Answer: [Yes].

Justification: We provide these information in the Appendices.

Guidelines:

- The answer [N/A] means that the paper does not include experiments.
- The paper should indicate the type of compute workers CPU or GPU, internal cluster, or cloud provider, including relevant memory and storage.
- The paper should provide the amount of compute required for each of the individual experimental runs as well as estimate the total compute.
- The paper should disclose whether the full research project required more compute than the experiments reported in the paper (e.g., preliminary or failed experiments that didn't make it into the paper).

#### 9. Code of ethics

Question: Does the research conducted in the paper conform, in every respect, with the NeurIPS Code of Ethics <https://neurips.cc/public/EthicsGuidelines>?

Answer: [Yes].

Justification: We followed the code of ethics.

Guidelines:

- The answer [N/A] means that the authors have not reviewed the NeurIPS Code of Ethics.
- If the authors answer [No], they should explain the special circumstances that require a deviation from the Code of Ethics.
- The authors should make sure to preserve anonymity (e.g., if there is a special consideration due to laws or regulations in their jurisdiction).

#### 10. Broader impacts

Question: Does the paper discuss both potential positive societal impacts and negative societal impacts of the work performed?

Answer: [No].

Justification: Our work is theoretically and empirically focused, without involving social impact.

Guidelines:

- The answer [N/A] means that there is no societal impact of the work performed.
- If the authors answer [N/A] or [No], they should explain why their work has no societal impact or why the paper does not address societal impact.
- Examples of negative societal impacts include potential malicious or unintended uses (e.g., disinformation, generating fake profiles, surveillance), fairness considerations (e.g., deployment of technologies that could make decisions that unfairly impact specific groups), privacy considerations, and security considerations.

- The conference expects that many papers will be foundational research and not tied to particular applications, let alone deployments. However, if there is a direct path to any negative applications, the authors should point it out. For example, it is legitimate to point out that an improvement in the quality of generative models could be used to generate Deepfakes for disinformation. On the other hand, it is not needed to point out that a generic algorithm for optimizing neural networks could enable people to train models that generate Deepfakes faster.
- The authors should consider possible harms that could arise when the technology is being used as intended and functioning correctly, harms that could arise when the technology is being used as intended but gives incorrect results, and harms following from (intentional or unintentional) misuse of the technology.
- If there are negative societal impacts, the authors could also discuss possible mitigation strategies (e.g., gated release of models, providing defenses in addition to attacks, mechanisms for monitoring misuse, mechanisms to monitor how a system learns from feedback over time, improving the efficiency and accessibility of ML).

## 11. Safeguards

Question: Does the paper describe safeguards that have been put in place for responsible release of data or models that have a high risk for misuse (e.g., pre-trained language models, image generators, or scraped datasets)?

Answer: [No].

Justification: We do not have such risks.

Guidelines:

- The answer [N/A] means that the paper poses no such risks.
- Released models that have a high risk for misuse or dual-use should be released with necessary safeguards to allow for controlled use of the model, for example by requiring that users adhere to usage guidelines or restrictions to access the model or implementing safety filters.
- Datasets that have been scraped from the Internet could pose safety risks. The authors should describe how they avoided releasing unsafe images.
- We recognize that providing effective safeguards is challenging, and many papers do not require this, but we encourage authors to take this into account and make a best faith effort.

## 12. Licenses for existing assets

Question: Are the creators or original owners of assets (e.g., code, data, models), used in the paper, properly credited and are the license and terms of use explicitly mentioned and properly respected?

Answer: [Yes].

Justification: We properly cited the datasets and LLMs analyzed.

Guidelines:

- The answer [N/A] means that the paper does not use existing assets.
- The authors should cite the original paper that produced the code package or dataset.
- The authors should state which version of the asset is used and, if possible, include a URL.
- The name of the license (e.g., CC-BY 4.0) should be included for each asset.
- For scraped data from a particular source (e.g., website), the copyright and terms of service of that source should be provided.
- If assets are released, the license, copyright information, and terms of use in the package should be provided. For popular datasets, [paperswithcode.com/datasets](https://paperswithcode.com/datasets) has curated licenses for some datasets. Their licensing guide can help determine the license of a dataset.
- For existing datasets that are re-packaged, both the original license and the license of the derived asset (if it has changed) should be provided.

- If this information is not available online, the authors are encouraged to reach out to the asset’s creators.

### 13. **New assets**

Question: Are new assets introduced in the paper well documented and is the documentation provided alongside the assets?

Answer: [N/A].

Justification: The paper does not release new assets.

Guidelines:

- The answer [N/A] means that the paper does not release new assets.
- Researchers should communicate the details of the dataset/code/model as part of their submissions via structured templates. This includes details about training, license, limitations, etc.
- The paper should discuss whether and how consent was obtained from people whose asset is used.
- At submission time, remember to anonymize your assets (if applicable). You can either create an anonymized URL or include an anonymized zip file.

### 14. **Crowdsourcing and research with human subjects**

Question: For crowdsourcing experiments and research with human subjects, does the paper include the full text of instructions given to participants and screenshots, if applicable, as well as details about compensation (if any)?

Answer: [N/A].

Justification: The paper does not involve crowdsourcing nor research with human subjects.

Guidelines:

- The answer [N/A] means that the paper does not involve crowdsourcing nor research with human subjects.
- Including this information in the supplemental material is fine, but if the main contribution of the paper involves human subjects, then as much detail as possible should be included in the main paper.
- According to the NeurIPS Code of Ethics, workers involved in data collection, curation, or other labor should be paid at least the minimum wage in the country of the data collector.

### 15. **Institutional review board (IRB) approvals or equivalent for research with human subjects**

Question: Does the paper describe potential risks incurred by study participants, whether such risks were disclosed to the subjects, and whether Institutional Review Board (IRB) approvals (or an equivalent approval/review based on the requirements of your country or institution) were obtained?

Answer: [N/A].

Justification: The paper does not involve crowdsourcing nor research with human subjects.

Guidelines:

- The answer [N/A] means that the paper does not involve crowdsourcing nor research with human subjects.
- Depending on the country in which research is conducted, IRB approval (or equivalent) may be required for any human subjects research. If you obtained IRB approval, you should clearly state this in the paper.
- We recognize that the procedures for this may vary significantly between institutions and locations, and we expect authors to adhere to the NeurIPS Code of Ethics and the guidelines for their institution.
- For initial submissions, do not include any information that would break anonymity (if applicable), such as the institution conducting the review.

### 16. **Declaration of LLM usage**

Question: Does the paper describe the usage of LLMs if it is an important, original, or non-standard component of the core methods in this research? Note that if the LLM is used only for writing, editing, or formatting purposes and does *not* impact the core methodology, scientific rigor, or originality of the research, declaration is not required.

Answer: [N/A].

Justification: The core method development in this research does not involve LLMs as any important, original, or non-standard components.

Guidelines:

- The answer [N/A] means that the core method development in this research does not involve LLMs as any important, original, or non-standard components.
- Please refer to our LLM policy in the NeurIPS handbook for what should or should not be described.